H2Open Journal

IWA PUBLISHING




H2Open Journal Vol 3 No 1
doi: 10.2166/h2oj.2020.010

# Removal of emerging persistent organic pollutants (Em-POPs) model compounds from water using a natural porous material functionalized with graphene-based products

Donald Boehm[a], Alice Lecus[a], Hai-Feng Zhang[b], David Garman[c] and Marcia R. Silva[a,*]

[a] Water Technology Accelerator (WaTA), University of Wisconsin-Milwaukee, 247 W. Freshwater Way, Milwaukee, Wisconsin 53204, USA

[b] AO Smith Corporation, One Park Plaza, 11270 W Park Pl #170, Milwaukee, Wisconsin 53224, USA

[c] Western Sydney University, 56 Second Avenue, Kingswood, NSW 2747, Australia

*Corresponding author. E-mail: msilva@uwm.edu

## Abstract

This study focuses on the removal of three model compounds, classified as emerging persistent organic pollutants (Em-POPs), from water using a modified version of natural Australian zeolite. Following a series of subsequent treatments and vacuum deposition of graphene oxide (GO), both chemical and physical properties of the adsorbent were characterized. The GO-coated zeolite was tested for the removal of methylene blue (MB), disperse blue 26 (DB26), and sodium fluorescein (NaFn). Results show excellent removal capability for MB and DB26 dyes and decent removal for NaFn when compared to commercially available products such as granular activated carbon. Regeneration of the adsorbent showed virtually no loss in adsorptive performance after two cycles, with MB and DB26.

**Key words:** dye, Em-POPs, graphene oxide, water remediation, zeolite

## Highlights

- Natural clinoptilolite-rich zeolite was successfully enhanced with graphene oxide to enhance surface properties.
- The vacuum graphene oxide coated zeolite was a successful method for deposition.
- Adsorption performance was improved by modification of the adsorbent for select dyes.
- The vacuum graphene oxide coated zeolite is competitive with other adsorbent materials on the market.
- Thermal stability of the precursor material is preserved throughout the treatment process.

## INTRODUCTION

Detection of many toxic and synthetically produced compounds in natural waters and other water supplies calls for improved methods for their removal due to their adverse health effects on humans and the ecosystem (Savage & Diallo 2005; WHO 2011). Out of the many compounds of interest, emerging persistent organic pollutants (Em-POPs) have been receiving a great deal of attention in recent years. This issue is particularly concerning for developing countries where locals consume and

H2Open Journal Vol 3 No 1
doi: 10.2166/h2oj.2020.010

utilize untreated water, but is prevalent all around the world (Wania & MacKay 1996; Ongley *et al.* 2010; Cincinelli *et al.* 2016; Rigét *et al.* 2016; Pozo *et al.* 2017; Unyimadu *et al.* 2017).

There are many compounds classified as POPs with varying levels of toxicity and volatility. Some common POPs include dyes, dioxins, furans, and polychlorinated biphenyls (PCBs), to name a few (Ritter *et al.* 2010; Yu *et al.* 2013). The most important attribute shared by all POPs is that they are persistent and that they are organic. These compounds are typically halogenated, usually with chlorine, containing highly stable C-Cl bonds. The increase in number of stable C-Cl bonds in a molecule also increases its resistance to degradation, in turn rendering them persistent in the environment (Ritter *et al.* 2010). PCBs for instance can remain in the environment for decades with minimal degradation.

Health hazards among POPs vary from molecule to molecule and it can be difficult to assign them to specific POP subgroups. Their toxicities are also variable, some are much less toxic than others while some can cause death from acute exposure (Ritter *et al.* 2010). Other common symptoms for POPs exposure include reproductive issues, endocrine disruption, diabetes, cardiovascular problems, and cacogenic responses (Ritter *et al.* 2010; Alharbi *et al.* 2018). Additionally, not all POPs exhibit these symptoms nor are these the only symptoms that can present themselves. One major issue behind POPs is that they bio-accumulate which can lead to high concentrations over time depending on exposure frequency and concentration (Alharbi *et al.* 2018).

Zeolite is a clay-based mineral that is both naturally occurring and can be synthetically produced. Both these materials have been proven to be an effective adsorbent in many studies (Khalid *et al.* 2004; Motsi *et al.* 2009; Mihaly-Cozmuta *et al.* 2014). The naturally occurring material is typically cheaper to obtain, however contains more imperfections in the zeolite lattice. This can be resolved by various treatment methods to achieve similar features of the synthetically produced variety. Two of the most important characteristics to consider include surface area and pore size because both features define the physical surface to which an adsorbate molecule can adsorb to. One successful method for tailoring natural zeolite includes acid treatment, which was shown to increase the surface area and decrease pore size (Silva *et al.* 2019, 2020).

In previous research, natural Australian zeolite (clinoptilolite) was coated with graphene oxide (GO) to enhance the surface properties of the material for the removal of cadmium from water showing adsorption capacities up to 720 $mg{\cdot}g^{-1}$ (Silva *et al.* 2020). Others have explored similar materials, including one that used the same raw materials used in this research, reporting adsorption capacities of 67.56 $mg{\cdot}g^{-1}$ for rhodamine b and 50 $mg{\cdot}g^{-1}$ for arsenic (Yu *et al.* 2013; Khatamian *et al.* 2017). In this study, natural Australian zeolite is modified to enhance the surface properties by acid treatment, which will be followed by vacuum deposition of GO in aqueous solution. This study will serve as preliminary research for the removal of Em-POPs from water using an engineered natural porous material for three Em-POPs model compounds: methylene blue (MB), disperse blue 26 (DB26), and sodium fluorescein (NaFn). It is expected that the combination of acid treatment followed by GO deposition will increase the surface area of the material which will also help to improve the material's adsorption capabilities. It is also expected that MB will have a higher affinity to the adsorbent material due to ionic attraction between the positively charged MB and the negatively charged GO. Understanding how charge effects the adsorption capabilities will help in fine-tuning the engineered material for removal of Em-POPs for future study. These dyes were also selected in the interest of using fewer toxic materials in addition to being relatively simple to analyze.

## METHODS

### Zeolite preparation

Australian natural zeolite (diameter: 0.7–1 mm, chemical composition: 68.26% $SiO_2$, 12.99% $Al_2O_3$, 4.11% $K_2O$, 2.09% CaO, 1.37% $Fe_2O_3$, 0.83% MgO, 0.64% $Na_2O$, 0.23% $TiO_2$) was provided by

H2Open Journal Vol 3 No 1
doi: 10.2166/h2oj.2020.010

Zeolite Australia Ltd. GO was produced from natural graphite powder (SP-1, Bay Carbon, MI, USA) using the modified Hummers' method (Mao *et al.* 2011). The GO suspension with a concentration of 2.5 g·mL$^{-1}$ was prepared by dispersing the prepared GO powder into deionized (DI) water with the assistance of ultrasonication for 10 min (Branson M1800 Ultrasonic Cleaner, 40 kHz). Other chemicals used in this study were sulfuric acid reagent grade 95–98% (Sigma Aldrich, USA) and ethyl-alcohol anhydrous (Electron Microscopy Sciences, USA), granular activated carbon (GAC, coconut carbon, Nichen #11268). Eighty grams of the natural zeolite was sonicated ten times in 15-minute intervals at 37 kHz in 1 L of deionized (DI) water, replacing the water between each interval. The zeolite was submerged in a 1:10 w/v ratio of DI water and microwaved to a low boil, repeating ten times and rinsing three times between each interval. Next, the zeolite was dried in an oven at 100 °C for 24 hours. This material will be referred to as clean zeolite throughout the paper. The clean zeolite was then added to a three-neck round-bottom flask with 460 mL of DI water and 40 mL of sulfuric acid using boiling chips. The necks of the flask were plugged with a rubber stopper, a punctured stopper containing a thermometer, and a Vigreux column. This was left on a heating mantle set to 90 °C for 12 hours. The flask was drained and the zeolite was rinsed using denatured anhydrous ethyl alcohol. The acid-treated zeolite was then placed in a beaker and dried at 100 °C for 24 hours. This dry material will be called acid-treated zeolite throughout the rest of this paper. Next, 15 g of acid-treated zeolite was mixed with 15 mL of 2.5 mg·mL$^{-1}$ GO solution in a beaker. The mixture was filtered using a vacuum-driven filter at 25 mm Hg for 10 minutes. The material was dried in an oven at 100 °C for 24 hours, and this will be called the vacuum GO (VGO)-coated sample.

### Zeolite characterization

Raman spectra were acquired on a Raman Microscope (Horiba Scientific Xplora Plus) with a 532 nm laser excitation, holographically ruled 1,800 grooves mm$^{-1}$ grating, using 100 × magnification. All Raman spectra were corrected for relative intensity using NIST SRM 2245. Fourier transform infrared spectroscopy (FTIR) spectra were recorded using an FTIR (Shimadzu, IRTracer-100) with an attenuated total reflectance (ATR) accessory (MIRacle 10, Single reflection ATR) with a resolution of 4 between 4,000 and 250 cm$^{-1}$. Laser power at the sample was 100 to 250 mW. Spectral processing was performed with LabSolutions IR. Thermogravimetric analysis (TGA) (Shimadzu Simultaneous DTA-TG Thermoanalyzer) used a heating rate of 5 °C min$^{-1}$ in air to a maximum temperature of 600 °C. The morphology and composition of the zeolite particles were characterized using scanning electron microscopy (SEM). Samples were mounted with conductive silver paste (EMSdiasum, 12686-15) on SEM stubs at 5 kV. The fabricated product was characterized by the determination of pore volume, surface area, and pore diameter using an automated gas sorption analyzer (Quantachrome autosorb iQ2) with ultra-high purity nitrogen gas. The surface area (SBET), pore size, and total pore volume distribution were determined by N2 adsorption isotherm with relationship between N2 adsorbed value at standard conditions (V) and the partial pressure ($p/p_0$) under −196 °C (ASAP 2020, Micromeritics Inst. Corp.). Samples were pre-treated by degassing at 150 °C for 2 hours, to remove adsorbed species. Pore size distributions were obtained by using the Barrett–Joyner–Halenda (BJH) method. Surface area calculations used the Brunauer–Emmett–Teller (BET) equation. Crystal structural features were determined using X-ray diffraction (XRD) (Bruker AXS).

### Column adsorption and regeneration experiments

Column experiments were performed to assess the adsorption capabilities of the zeolite. Experiments were set up to utilize a 1.5 cm diameter column, 20 cm in length (Synthware), 10 cm bed height, with a mini-pump (Control Company mini-pump, variable flow). A cotton gauze layer of about 1 cm was placed at the bottom of the column to prevent the zeolite from clogging the stopcock. One liter of

H2Open Journal Vol 3 No 1
doi: 10.2166/h2oj.2020.010

tap water was flushed through the columns or until the effluent pH was 7 ± 0.5. The columns were conducted with a flow rate of 0.08 (±0.03) mL·s$^{-1}$ with monitoring of pH of all effluent. MB, DB26, and NaFn were used as model compounds for these subsequent experiments at 40 mg·L$^{-1}$ concentrations. These compounds were selected as model compounds with different charge properties of cationic, anionic, and non-ionic organic molecules. Columns were run for a total of 16 pore volumes, defined by the void space between the adsorbent and the column. MB and DB dye samples were analyzed using a UV Vis Spectrophotometer (Evolution) and the NaFn was analyzed using a Synergy H4 Hybrid Reader equipped with Gen5 2.04 software. All tests were conducted in triplicate. Solution volume was defined by taking the sum of all of the aliquot concentrations following the removal efficiency equation as follows:

$$R\ (\%) = \frac{C_0 - C_e}{C_0} \times 100 \tag{1}$$

where $C_0$ and $C_e$ are the dye concentrations (mg·L$^{-1}$) in the aqueous phase before and after sorption, respectively.

The regeneration of the material containing the absorbed dyes was undertaken in a rotary furnace (STTR-1200C-3-12, SentroTech) for 5 hours at 550 °C without rotation. The material was placed in a ceramic boat prior to loading it inside the furnace. Adsorption performance for MB and DB26 dyes were examined after each of the three regeneration cycles. Experiments were run in triplicate for MB, except for the final replicate on the third regeneration cycle. The regeneration experiments for DB26 were repeated in duplicate. Removal efficiency was calculated according to Equation (1).

### Zeta potential analysis

Zeta potential was examined for all three dye solutions and for the surface of the VGO zeolite. The dyes were prepared at 40 mg/L concentrations in the pH range of 3.5 and 7.5, which were then measured on a Malvern Zetasizer Nano using a DTS 1070 cuvette. The VGO zeolite was added to three separate beakers containing 20 mL of DI water and the pH of the solution was adjusted to be within the range used for the dye solutions. All the VGO zeolite was added to the cuvette and was filled with the pH adjusted solution. All pH adjustments were made using sodium hydroxide and hydrochloric acid solutions.

### Quantification of GO

To assess the loss of GO during filtration, material was column leached with deionized water (60 mL). The effluent was filtered (Whatman 0.2 μm pore size 25 mm diameter; 25 mm Hg; Supelco). GO solutions were filtered onto membranes as calibration standards. Calibration standards and the samples were dried at room temperature for 24 hours. Membranes were mounted onto aluminum specimen mounts (Ted Pella INC, Hitachi M4) using double-sided carbon adhesive tabs (Lift-N-Press). The membranes were grounded to the mount using a strip of conductive double-sided copper tape (3 M). Two nanometers of iridium were surface coated using a sputter coater (Emitech, K575X) and analyzed by scanning electron microscope (Hitachi S-4800). Semi-quantitative comparisons of the images of the various mounts were made to determine the maximum potential concentration of GO per sample solution.

H2Open Journal Vol 3 No 1
doi: 10.2166/h2oj.2020.010

## RESULTS AND DISCUSSION

### Characterization of zeolite

Spectral data obtained from Raman (Figure 1) confirm the presence of GO on the surface of the sample. This can be confirmed by the presence of the predominant G peak at 1,580 $cm^{-1}$ and the D peak at 1,340 $cm^{-1}$ (Yang *et al.* 2009). The spectra for the clean zeolite show a considerably different spectra in the GO region, which may be attributed to zeolite blocking by the deposited GO or because of the variation in the zeolite composition. Another study that examined the Raman spectra of GO-coated zeolite found very similar results (Yu *et al.* 2013). The G and D bands provide important information about the structural order of GO; these correspond to the disorder and stacking of the nanosheets. The $E_{2G}$ vibrational mode of first order Raman scattering is represented by the G band while the D band is attributed to the disorder and asymmetric bonding throughout the graphitic plane (Sutar *et al.* 2012).

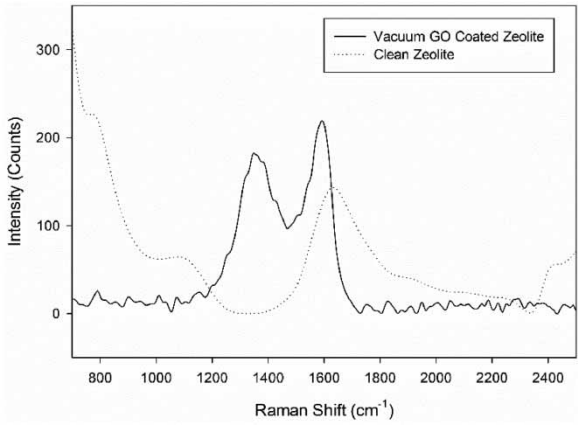


**Figure 1** | Raman spectra of the clean zeolite and the VGO-coated zeolite. The data confirm the presence of GO on the surface of the zeolite at the end of the treatment process.

Information about the zeolites IR active bands were examined using FTIR with an ATR configuration. The most significant peak that appears in IR spectrum corresponds to $SiO_2$ at 1,205 $cm^{-1}$. Figure 2(a) shows the IR spectra of the GO-coated zeolite before and after TGA. The signal flux is likely due to variability among replicates and samples, the relative ratios remained the same. One peak around 2,400 $cm^{-1}$ was found in the GO-coated sample that disappeared after TGA indicating

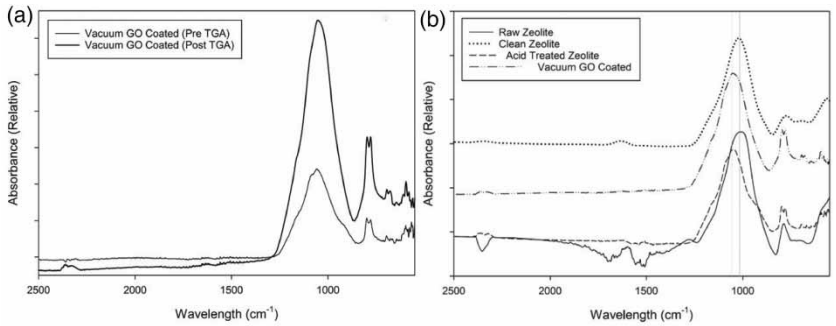


**Figure 2** | (a) FTIR of GO-coated zeolite before and after TGA showing that the treated material retains the same thermal properties as the precursor material at 600 °C. (b) FTIR of the GO-coated zeolite and its precursor materials showing a slight shift at 1,200 $cm^{-1}$ indicating the dealumination of zeolite.

H2Open Journal Vol 3 No 1
doi: 10.2166/h2oj.2020.010

water evaporation. Peaks associated with GO were not observed in the IR region and this may be due to either the amount of GO deposition or the GO itself. These data suggest that the zeolite does not lose its thermal stability throughout the coating method.

This however does not suggest that the zeolite was not substantially altered throughout the treatment process. Figure 2(b) shows a slight shift in the peak around 1,200 $cm^{-1}$ to higher wavelengths, indicating a change in between the clean zeolite and the acid-treated zeolite. This has been reported by other authors to be a result of dealuminating the zeolite (Garcia-Basabe *et al.* 2010). FTIR results are also in agreement with the TGA data and confirmed that zeolite retained its thermal stability.

Changes in crystallinity were not observed by X-ray diffraction. It was suspected that any changes would likely occur as a result of dealumination from acid treatment which was not the case. It is likely that any slight differences result from experimental error.

Results from TGA analysis in Figure 3 show only slight variation between the different stages of GO deposition. The clean and acid-treated zeolite particles lost 1–2% more of their masses compared to the vacuum-coated zeolite. This confirms that the treated zeolite is still able to retain most if not all of its thermal stability throughout the various stages of treatments. The data suggest that the GO remains on the surface after being exposed to temperatures up to 600 °C. Other studies found similar results and one reported that combustion begins to occur at temperatures closer to 650 °C (Guadagno *et al.* 2015; Sharma *et al.* 2018). Thermal stability of GO was not affected within the range of temperature of our study.

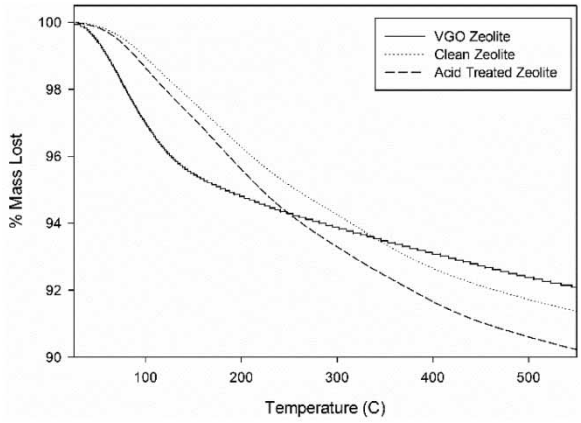


**Figure 3** | TGA of clean, acid-treated, and VGO-coated zeolite samples.

Detailed analysis of the surface features was carried out by SEM to confirm macroscopic observations about the evenness of GO using the vacuum coating method. Figure 4(a) shows the

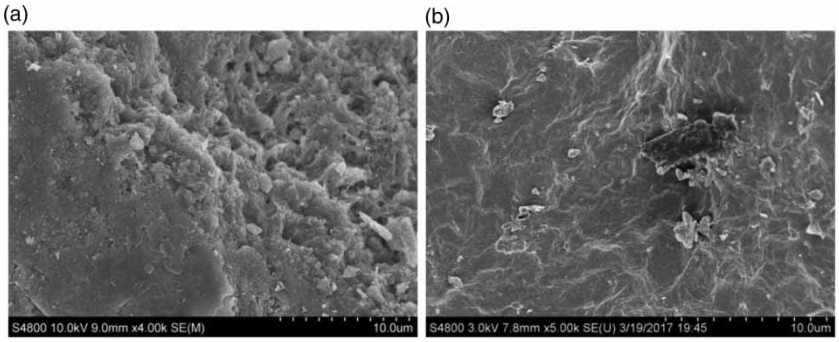


**Figure 4** | (a) SEM image of acid-treated zeolite. Sharp features can be observed. (b) SEM image of GO-coated zeolite. The large darker sheet-like areas of the image correspond to the deposition of GO on the surface of the zeolite.

H2Open Journal Vol 3 No 1
doi: 10.2166/h2oj.2020.010

features of the acid-treated sample where sharp ridges and rough surface can be seen. The vacuum GO-coated zeolite shows these features as well, but also includes dark islands of GO unevenly scattered across the surface (Figure 4). High magnification of the GO-coated regions show wrinkly features, indicating the presence of GO sheets. Figure 4(b) also shows substantially more charging, which is likely due to the electron beam 'lighting up' the edges of the GO sheets (Zhou *et al.* 2016). These dark spots were not observed in the acid-treated or clean zeolite (not shown) samples. Aside from the highly visible GO islands, it is likely that there are more GO-coated regions than can be seen; the main issue in resolving an image of GO by SEM is due to the low electron density of carbon. The secondary electrons can penetrate through the GO sheets to the substrate, where only the substrate can be seen (Hassink *et al.* 2015). The deposition is undoubtedly non-uniform, an observation that can be confirmed both macroscopically and microscopically.

The surface area and the pore size of the samples were determined using gas sorption analysis. This information allows the analyst to determine the theoretical surface to which an adsorbate molecule can bind. Achieving the highest possible surface area is, therefore, fundamentally important because it will help define the physical limits of adsorption. The VGO-coated zeolite sample had a surface area of 89.4 $m^2 \cdot g^{-1}$ and pore size of 5.95 Å, which was similar to results found for the acid-treated sample with a surface area of 86.13 $m^2 \cdot g^{-1}$ and pore size of 30.47 Å (single sample measurements for both). The raw zeolite and clean zeolite samples show much lower surface areas and larger pore sizes than the VGO sample. The average surface area for the raw material was 13.15 $m^2 \cdot g^{-1}$ with an average pore size of 76.37 Å, the clean zeolite had an average surface area of 10.56 $m^2 \cdot g^{-1}$ with an average pore size of 81.91 Å (both measured in triplicate). Acid treatment simultaneously increases the surface area and decreases the pore size of the material to 81.55 $m^2/g$ and 29.90 Å, respectively. From the data obtained, the VGO-coated sample showed that the majority of the pores fall below 20 Å, and are classified as micropores according to the International Union of Pure and Applied Chemistry (IUPAC) classification of pores. The decrease in pore size for the VGO sample can be attributed to pore blocking by GO. The adsorption and desorption isotherms (not included in this paper) show the best correlation to hysteresis of the type 4, which supports pore blocking. Under the IUPAC classification of hysteresis loops, the type 4 adsorption branch is a combination of types 1 and 2; the type 2 isotherm is associated with pore blocking. The surface area for the VGO-coated zeolite shows a substantial increase departing from the raw material, shown in Figure 5. These data suggest that the method of vacuum coating was successfully able to enhance the zeolite surface area and reduce the pore size.

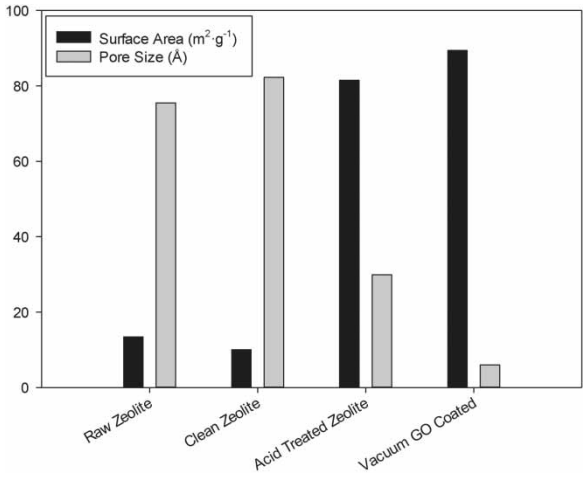


**Figure 5** | Gas sorption data for raw, clean, acid-treated, and VGO-coated zeolites. This graph shows the correlation between each step in the fabrication process and how it impacts the surface area and porosity; results reported as single measurements.

H2Open Journal Vol 3 No 1
doi: 10.2166/h2oj.2020.010

Data obtained using model compounds MB, DB26, and NaFn showed favorable results for the VGO-coated zeolite samples (Figure 6). When running columns with MB, the GO-coated zeolite only slightly outperformed the clean zeolite and the GAC sample with removal percentages of 100, 98, and 99%, respectively. Columns with DB26 still showed good results for the GO-coated zeolite, however the overall adsorptive performance was reduced for all three adsorbent materials. The removal percentages for VGO-coated zeolite, clean zeolite, and GAC were 68, 6, and 67%, respectively. While the VGO-coated zeolite exhibited higher removal than the clean zeolite when running columns with NaFn, the GAC performed the best (with removal percentages of 63, 14, and 76%, respectively). The best results for dye removal using the VGO zeolite were obtained by MB, then DB26 and NaFn, respectively. It is highly likely that this is due to the ionic nature of the dyes, MB is cationic and therefore better able to bind to the negatively charged GO. Removal efficiency is decreased for the non-ionic DB26 and further decreased for NaFn. Breakthrough curves can be found in Figure 6 in addition to pH records throughout the experiments. Adjustments in pH of the VGO-coated zeolite could lead to significant improvements in the performance of the adsorbent (Bailey *et al.* 1968; Kim 2010). The pH trends for the column experiments were variable across all three dyes, ranging roughly from 3 to 7. The lowest pH values come from the MB experiments (close to pH = 3.5), the highest was obtained from NaFn (slightly over pH = 5), and the pH values for the DB26 trials were slightly less (pH = 5). The changes in pH are likely due to equilibrium being reached in the column following the initial contact of adsorbate and adsorbent. Change in pH is most profound for the NaFn experiment where there is an initial increase in pH for the first three pore volumes, until it gradually decreases afterwards. A similar trend can be observed in the breakthrough curves for the DB26 and NaFn columns, where the removal efficiency is initially

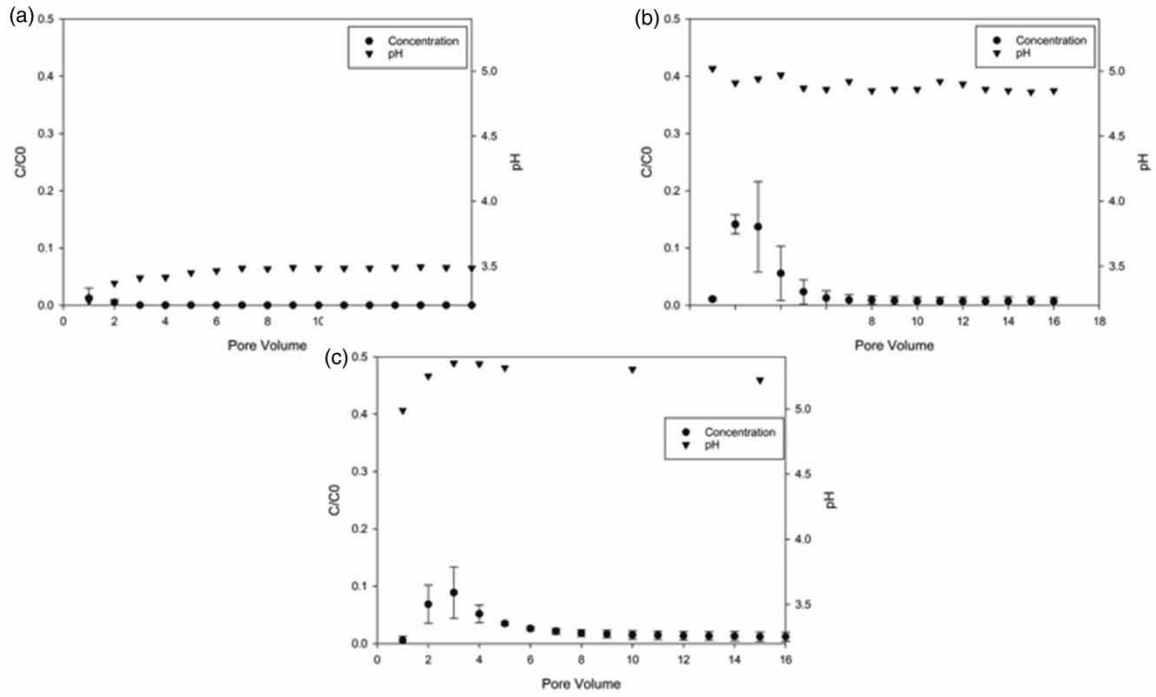


**Figure 6** | (a) Breakthrough curve showing MB passing through a GO-coated zeolite column with corresponding pH values for each sample. Minimal initial breakthrough followed by complete retention shows that the adsorptive potential for this dye is very high. (b) Breakthrough curve showing DB penetration through a GO-coated zeolite column with corresponding pH values for each sample. Initial breakthrough was moderate. However, since later samples in the column show a very low concentration, the overall retention of the dye was within a similar range to GAC. (c) Breakthrough curve showing NaFn passing through a GO-coated zeolite column with corresponding pH values for each sample. Concentrations of the samples were elevated throughout and showed adsorptive performance slightly lower, but comparative to what would be expected for GAC.

H2Open Journal Vol 3 No 1
doi: 10.2166/h2oj.2020.010

reduced before it is improved after the third pore volume. Further testing at various pH conditions and concentrations would be needed in order to fully understand this trend.

Results from the MB columns showed high removal for all three adsorbents; however, each material is different. Both the VGO zeolite and GAC are amphoteric carbon-based materials with hydroxyl-rich surfaces that can be either protonated or deprotonated. Zeolites naturally contain a higher amount of negatively charged functional groups at the surface, requiring treatment for the inclusion of more positive groups. The data obtained for DB26 from the VGO zeolite and GAC columns show substantially higher removal than for clean zeolite, and a similar trend can be observed for NaFn. The results suggest that electrostatic interactions significantly influence the adsorption of these dyes and is supported by zeta potential analysis.

The zeta potential for all three dyes at 40 mg/L (pH ~3.5, 4, and 7) were tested in addition to the VGO zeolite (Figure 7). Methylene blue, a cationic dye, showed a positive increase in zeta potential at a pH slightly above 4, while the opposite occurs for the VGO zeolite at relatively similar pH values. The lowest zeta potential values were obtained from the DB26 samples with the lowest value of −51.5 mV and is substantially less than the results obtained for NaFn. Comparing these results to the data obtained from the column experiments reveals a correlation between zeta potential and dye adsorption. The DB26 samples showed the lowest zeta potential values and the lowest removal for clean zeolite. While both the VGO zeolite and GAC can become protonated or deprotonated, the clean zeolite does not contain nearly as many positive sites to attract the negative charge. While still negatively charged, results for the NaFn and clean zeolite show improvement where the removal was more than doubled. The zeta potential trend for NaFn was substantially less negative than for the DB26 column.

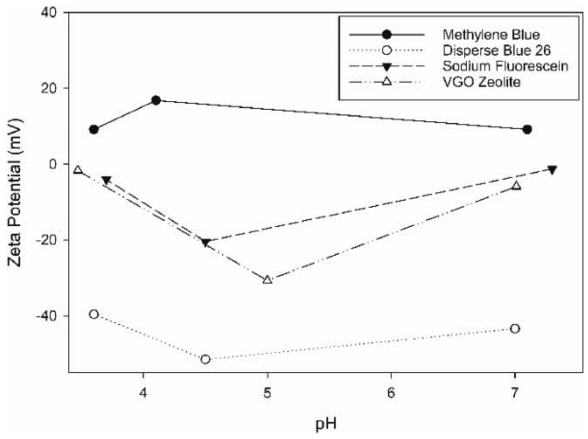


**Figure 7** | The data from the zeta potential results for MB, DB26, NaFn, and VGO zeolite at varying pH.

In addition to electrostatic interactions, the surface area and pore size of the adsorbents have a substantial impact on adsorption properties. Departing from the clean zeolite, the surface area is increased when the material is acid treated and is further increased after GO deposition. The increase in surface area occurs while the pore size is decreased as a result of dealumination in the acid treatment step, followed by pore blocking from GO coating. Increasing surface area is critical for optimum adsorption performance because it will also increase the amount of adsorbate able to bind to the surface of the adsorbent. The data show that GO deposition not only increases surface area, but also suggests that it improves adsorption through a process dominated by electrostatic interactions at optimal pH.

In most of the regeneration trials that were performed using either MB or DB26 dyes, adsorptive performance is retained for at least two subsequent regenerations as shown in Figure 8. Based on

H2Open Journal Vol 3 No 1
doi: 10.2166/h2oj.2020.010

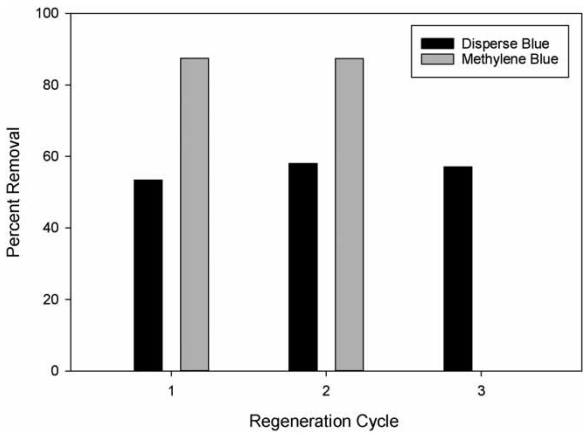


**Figure 8** | Regeneration results from using the VGO-coated zeolite using DB26 and MB dyes. The adsorbent shows better removal of MB than DB26. Data for the third cycle using MB were not available.

the trend shown, it is believed that the material would also likely retain its properties for three or more regenerations, however further testing would be needed to confirm this. This indicates that this material is resistant to high temperature treatments for thermal regeneration and can be reused. Furthermore, these results show potential for this material to be used as a commercial adsorbent.

## CONCLUSIONS

Results from zeolite characterization show improved features departing from the original material. Both Raman and SEM analysis of the VGO-coated sample confirms the deposition of GO on the surface of the zeolite. FTIR shows that the material was successfully dealuminated by acid treatment in addition to the material retaining its thermal properties throughout the treatment process. This was also complemented by TGA results which showed that the material retained most if not all its original thermal stability. XRD did not show any changes in the material's structural order, which would have been expected for acid-treated samples. Gas sorption analysis showed that acid treatment followed by VGO deposition both increases the surface area and reduces the pore size. The overall process was successful in its efforts to improve surface features to enhance adsorption performance.

Adsorption experiments show that the VGO-coated zeolite can be a competitive adsorbent for MB and DB26 dyes. While the material was able to remove 63% of NaFn, the GAC sample performed slightly better by 13% higher removal. Regeneration of the adsorbent shows that at least two cycles are possible for MB and DB26 dyes, however further examination is needed to determine the limitations of the adsorbent. Results from zeta potential analysis indicate that electrostatic interactions play a critical role in the adsorption process. Additionally, this adsorbent must be tested with Em-POPs to fully understand the potential of this material for this application. The VGO-coated zeolite shows promise as a suitable adsorbent for the removal of model compounds MB and DB26 and therefore for the removal of Em-POPs as well.

## ACKNOWLEDGEMENTS

The authors thank Dr Heather A. Owen for technical support with SEM analyses at the UWM Electron Microscope Laboratory; Angela Schmoldt from the UWM Genomics Center, School of Freshwater Sciences for technical assistance with Synergy H4 Hybrid Reader for sodium fluorescein analysis; and Dr Steve Hardcastle from UWM Advanced Analytical Facility (AAF) for assistance with

H2Open Journal Vol 3 No 1
doi: 10.2166/h2oj.2020.010

BET and XRD analysis. This research study was supported by the National Science Foundation Industry/University Cooperative Research Center on Water Equipment & Policy located at University of Wisconsin-Milwaukee (IIP-1540032) and Marquette University (IIP-1540010).

## DATA AVAILABILITY STATEMENT

All relevant data are included in the paper or its Supplementary Information.

## REFERENCES

Alharbi, O. M. L., Basheer, A. A., Khattab, R. A. & Ali, I. 2018 Health and environmental effects of persistent organic pollutants. *Journal of Molecular Liquids* **263**, 442–453.

Bailey, G. W., White, J. L. & Rothberg, T. 1968 Adsorption of organic herbicides by montmorillonite: role of pH and chemical character of adsorbate. *Soil Science Society of America Journal* **32**, 222–234.

Cincinelli, A., Martellini, T., Pozo, K., Kukučka, P., Audy, O. & Corsolini, S. 2016 Trematomus bernacchii as an indicator of POP temporal trend in the Antarctic seawaters. *Environmental Pollution* **217**, 19–25.

Garcia-Basabe, Y., Rodriguez-Iznaga, I., de Menorval, L.-C., Llewellyn, P., Maurin, G., Lewis, D. W., Binions, R., Autie, M. & Ruiz-Salvador, A. R. 2010 Step-wise dealumination of natural clinoptilolite: structural and physicochemical characterization. *Microporous and Mesoporous Materials* **135** (1), 187–196.

Guadagno, L., Raimondo, M., Vertuccio, L., Mauro, M., Guerra, G., Lafdi, K., De Vivo, B., Lamberti, P., Spinelli, G. & Tucci, V. 2015 Optimization of graphene-based materials outperforming host epoxy matrices. *RSC Advances* **5** (46), 36969–36978.

Hassink, G., Wanke, R., Rastegar, I., Braun, W., Stephanos, C., Herlinger, P., Smet, J. H. & Mannhart, J. 2015 Transparency of graphene for low-energy electrons measured in a vacuum-triode setup. *APL Materials* **3** (7), 076106.

Khalid, M., Joly, G., Renaud, A. & Magnoux, P. 2004 Removal of phenol from water by adsorption using zeolites. *Industrial & Engineering Chemistry Research* **43** (17), 5275–5280.

Khatamian, M., Khodakarampoor, N. & Saket-Oskoui, M. 2017 Efficient removal of arsenic using graphene-zeolite based composites. *Journal of Colloid and Interface Science* **498**, 433–441.

Kim, M.-J. 2010 Effects of pH, adsorbate/adsorbent ratio, temperature and ionic strength on the adsorption of arsenate onto soil. *Geochemistry Exploration Environment Analysis* **10** (4), 407–412.

Mao, S., Yu, K. H., Cui, S. M., Bo, Z., Lu, G. H. & Chen, J. H. 2011 A new reducing agent to prepare single-layer, high-quality reduced graphene oxide for device applications. *Nanoscale* **3**, 2849–2853.

Mihaly-Cozmuta, L., Mihaly-Cozmuta, A., Peter, A., Nicula, C., Tutu, H., Silipas, D. & Indrea, E. 2014 Adsorption of heavy metal cations by Na-clinoptilolite: equilibrium and selectivity studies. *Journal of Environmental Management* **137**, 69–80.

Motsi, T., Rowson, N. A. & Simmons, M. J. H. 2009 Adsorption of heavy metals from acid mine drainage by natural zeolite. *International Journal of Mineral Processing* **92** (1), 42–48.

Ongley, E. D., Xiaolan, Z. & Tao, Y. 2010 Current status of agricultural and rural non-point source pollution assessment in China. *Environmental Pollution* **158** (5), 1159–1168.

Pozo, K., Sarkar, S. K., Estellano, V. H., Mitra, S., Audi, O., Kukucka, P., Přibylová, P., Klánová, J. & Corsolini, S. 2017 Passive air sampling of persistent organic pollutants (POPs) and emerging compounds in Kolkata megacity and rural mangrove wetland Sundarban in India: an approach to regional monitoring. *Chemosphere* **168**, 1430–1438.

Rigét, F., Vorkamp, K., Bossi, R., Sonne, C., Letcher, R. J. & Dietz, R. 2016 Twenty years of monitoring of persistent organic pollutants in Greenland biota. A review. *Environmental Pollution* **217**, 114–123.

Ritter, L., Solomon, K. R. & Forget, J. 2010 *Persistent Organic Pollutants an Assessment Report on: DDT-Aldrin-Dieldrin-Endrin-Chlordane, Heptachlor-Hexachlorobenzene, Mirex-Toxaphene, Polychlorinated Biphenyls, Dioxins and Furans*. International Programme on Chemical Safety.

Savage, N. & Diallo, M. S. 2005 Nanomaterials and water purification: opportunities and challenges. *Journal of Nanoparticle Research* **7** (4), 331–342.

Sharma, S., Susan, D., Kothiyal, N. C. & Kaur, R., 2018 Graphene oxide prepared from mechanically milled graphite: effect on strength of novel fly-ash based cementitious matrix. *Construction and Building Materials* **177**, 10–22.

Silva, M., Lecus, A., Lin, Y. & Corrao, J. 2019 Tailoring natural zeolites by acid treatments. *Journal of Materials Science and Chemical Engineering* **7**, 26–37.

Silva, M. R., Lecus, A., Gajdardziska-Josifovska, M., Schofield, M., Virnoche, M., Chang, J., Chen, J. & Garman, D. 2020 Graphene-oxide loading on natural zeolite particles for enhancement of adsorption properties. *RSC Advances* **10** (8), 4589–4597.

Sutar, D. S., Narayanam, P. K., Singh, G., Botcha, V. D., Talwar, S. S., Srinivasa, R. S. & Major, S. S. 2012 Spectroscopic studies of large sheets of graphene oxide and reduced graphene oxide monolayers prepared by Langmuir–Blodgett technique. *Thin Solid Films* **520** (18), 5991–5996.

H$_2$Open Journal Vol 3 No 1
doi: 10.2166/h2oj.2020.010

Unyimadu, J. P., Osibanjo, O. & Babayemi, J. O. 2017 Selected persistent organic pollutants (POPs) in water of River Niger: occurrence and distribution. *Environmental Monitoring and Assessment* **190** (1), 6.

Wania, F. & MacKay, D. 1996 Peer reviewed: tracking the distribution of persistent organic pollutants. *Environmental Science & Technology* **30** (9), 390A–396A.

WHO 2011 *Pharmaceuticals in Drinking Water*. World Health Organization, Geneva, Switzerland.

Yang, D., Velamakanni, A., Bozoklu, G., Park, S., Stoller, M., Piner, R. D., Stankovich, S., Jung, I., Field, D. A., Ventrice, C. A. & Ruoff, R. S. 2009 Chemical analysis of graphene oxide films after heat and chemical treatments by X-ray photoelectron and Micro-Raman spectroscopy. *Carbon* **47** (1), 145–152.

Yu, Y., Murthy, B. N., Shapter, J. G., Constantopoulos, K. T., Voelcker, N. H. & Ellis, A. V. 2013 Benzene carboxylic acid derivatized graphene oxide nanosheets on natural zeolites as effective adsorbents for cationic dye removal. *Journal of Hazardous Materials* **260**, 330–338.

Zhou, Y., Fox, D. S., Maguire, P., O'Connell, R., Masters, R., Rodenburg, C., Wu, H., Dapor, M., Chen, Y. & Zhang, H. 2016 Quantitative secondary electron imaging for work function extraction at atomic level and layer identification of graphene. *Scientific Reports* **6**, 21045.

First received 3 February 2020; accepted in revised form 14 August 2020. Available online 14 October 2020